Journal of Peptide Science
J. Pept. Sci. 2008; **14**: 192–202
Published online 26 November 2007 in Wiley InterScience (www.interscience.wiley.com). DOI: 10.1002/psc.974

JOURNAL OF PEPTIDE SCIENCE

Distance dependence of long-range electron transfer through helical peptides‡

MINAKO KAI, KAZUKI TAKEDA, TOMOYUKI MORITA and SHUNSAKU KIMURA*

Department of Material Chemistry, Graduate School of Engineering, Kyoto University, Kyoto-Daigaku-Katsura, Nishikyo-ku, Kyoto 615-8510, Japan

Received 7 June 2007; Revised 28 September 2007; Accepted 10 October 2007

Abstract: Helical peptides of 8mer, 16mer, and 24mer carrying a disulfide group at the *N*-terminal and a ferrocene moiety at the *C*-terminal were synthesized, and they were self-assembled on gold by a sulfur–gold linkage. Infrared reflection–absorption spectroscopy and ellipsometry confirmed that they formed a monolayer with upright orientation. Cyclic voltammetry showed that the electron transfer from the ferrocene moiety to gold occurred even with the longest 24mer peptide. Chronoamperometry and electrochemical impedance spectroscopy were carried out to determine the standard electron transfer rate constants. It was found that the dependence of the electron-transfer rates on the distance was significantly weak with the extension of the chain from 16mer to 24mer (decay constant $\beta = 0.02–0.04$). This dependence on distance cannot be explained by an electron tunneling mechanism even if increased hydrogen-bonding cooperativity or molecular dynamics is considered. It is thus concluded that this long-range electron transfer is operated by an electron hopping mechanism. Copyright © 2007 European Peptide Society and John Wiley & Sons, Ltd.

Keywords: helical peptide; ferrocene; disulfide; self-assembled monolayer; gold; electrochemistry; electron transfer; hopping mechanism

INTRODUCTION

Electron transfer though peptide secondary structures has been of great interest for clarifying efficient electron-transfer reactions occurring in protein assemblies in nature [1–5]. Especially, electron transfer through helices has attracted much attention because it is believed that α-helical segments play an essential role in mediating an electron and determining its direction in biological systems [6]. To study the nature of electron transfer, radiolysis [7,8] and photoinduced electron-transfer [9] studies in solution (donor–peptide–acceptor), electrochemical studies on self-assembled monolayer (SAM) systems (donor–peptide–metal) [10–15], and recently, single molecule measurements by scanning probe microscopy (metal–peptide–metal) [16–18], have been conducted intensively. Most of the researchers agree that a helical peptide is a good electron mediator and enables electron transfer over a long distance. Yet, there has been a controversy over its mechanism [19]. There are two mechanisms. One is an electron tunneling mechanism by the electronic coupling between the donor and acceptor virtually through the molecular orbitals of the peptide bridge. The other is an electron hopping mechanism in which a charge (electron or hole) is first injected from the donor or acceptor to the peptide bridge and then it hops through the peptide bridge to reach the acceptor or donor. The electron-transfer rate decays exponentially with the increase of distance in the tunneling, while it is inversely proportional to the distance in the hopping [20]. To avoid confusion about the mechanism, one should keep it in mind that the both mechanisms are available but the dominant mechanism is changeable depending on the electron-transfer distance and the reaction driving force of the molecular system. The driving force is the difference in the redox potentials of the donor and acceptor (Fermi level in the case of metal). When the electron-transfer distance is short or the driving force is large, tunneling prevails. Sisido and co-workers investigated photoinduced electron transfer from pyrene to nitrobenzene separated by 0–8 cyclohexyl glutamate residues, and found that the electron-transfer rate decayed exponentially with the distance with a decay factor (β) of 0.66 $Å^{-1}$ [9]. Maran and co-workers studied electrochemically induced electron transfer in a donor-$(Aib)_n$-acceptor system ($n = 0–6$; Aib = α-aminoisobutyric acid) and suggested that the electron transfer occurred by tunneling, and increased cooperativity of hydrogen bonds with chain elongation was responsible for the observed weak distance dependence [21,22]. Tao and co-workers measured single molecule conductances of a series of cysteamine-$(Gly)_n$-Cys peptides ($n = 0–2$, not helical peptide) in a gold–peptide–gold junction by their scanning tunneling microscopy and concluded that tunneling was operative with β of 0.87 $Å^{-1}$ [16]. Using the same method, Sek and co-workers reported a similar

*Correspondence to: Shunsaku Kimura, Department of Material Chemistry, Graduate School of Engineering, Kyoto University, Kyoto-Daigaku-Katsura, Nishikyo-ku, Kyoto 615-8510, Japan;
e-mail: shun@scl.kyoto-u.ac.jp

‡This article is part of the Special Issue of the Journal of Peptide Science entitled "Peptides in Nanotechnology".

tunneling behavior for Ala-rich 14mer to 17mer peptides with β of 0.50 $Å^{-1}$ [18]. Their peptides were long but they were substantially tilted on the gold surface, where the shortcut distance along the surface normal was 18–21 Å, implying to be in the distance range of tunneling. On the other hand, when a peptide bridge is long and the driving force is small, a hopping mechanism should take over tunneling. Isied and co-workers carried out radiolysis and photolysis experiments on a donor-$(Pro)_n$-acceptor system ($n = 0$–9) and observed a dramatic transition in β values from 1.4 to 0.18 $Å^{-1}$ when the donor–acceptor separation was over 20 Å [23]. They attributed the anomalously weak distance dependence to a hopping mechanism. In our previous work, we prepared SAMs of 16mer (Leu-Aib) or 18mer (Ala-Aib) helical peptides carrying a ferrocene moiety at the terminal, and investigated the electron transfer from the ferrocene moiety to gold by electrochemistry [10,11]. The separation between the ferrocene moiety and gold was quite long (even the shortcut distance was over 25 Å) and the driving force was zero (the rate constants when the ferrocene oxidation potential equaled to the gold Fermi level were discussed). We found that the experimental rate constants were 10^3–10^4 times larger than the theoretical rate based on the tunneling mechanism. We thus suggested that a hopping mechanism with amide groups as hopping sites was responsible for this long-range electron transfer. Kraatz and co-workers studied a similar monolayer system with Pro-based peptides carrying a ferrocene moiety at the terminal, and they observed a very weak distance dependence that could be attributed to hopping [12,13]. Recently, however, they have emphasized the importance of molecular dynamics whether the electron transfer is governed by tunneling or hopping [14].

In this study, we discuss the distance dependence up to a 24mer peptide, which, to the best of our knowledge, is the longest peptide bridge ever studied for electron transfer. Three helical peptides having an alternating Ala-Aib sequence with three different lengths (8mer, 16mer, and 24mer) were used (SSA8Fc, SSA16Fc, and SSA24Fc; Figure 1). Each peptide had a disulfide group at the *N*-terminal for immobilization onto gold, and a ferrocene moiety at the *C*-terminal. They were self-assembled on gold by a sulfur-gold linkage. Infrared reflection–absorption spectroscopy (IRRAS) and ellipsometry indicated that they formed a monolayer with upright orientation. The electron transfer from the ferrocene moiety to gold was studied by electrochemical methods including cyclic voltammetry (CV), chronoamperometry (CA), and electrochemical impedance spectroscopy (EIS). The results suggested that the electron transfer in the 8mer peptide might be operated by a tunneling mechanism; on the other hand, a hopping mechanism should be dominant for the electron transfer in the 16mer and 24mer peptides. We also discuss the potential effects of hydrogen-bonding cooperativity and molecular dynamics proposed by the other researchers.

MATERIALS AND METHODS

Synthesis of Helical Peptides

SSA8Fc, SSA16Fc, and SSA24Fc were synthesized by the conventional liquid-phase method. Boc-$(Ala\text{-}Aib)_4$-OBzl and Boc-$(Ala\text{-}Aib)_8$-OBzl were synthesized according to the method reported in the literature [24] where Boc stands for *tert*-butyloxycarbonyl and OBzl for benzyl ester. Chemical modifications of the peptides (8mer and 16mer) with the ferrocene moiety at the *C*-terminal and lipoic acid at the *N*-terminal were done similar to our previous work [10]. Briefly, the OBzl group at the *C*-terminal was first removed by the catalytic hydrogenation in dichloromethane with 15 wt% palladium carbon under a H_2 atmosphere, and an ethylenediamine-modified ferrocene derivative ($NH_2CH_2CH_2NHCO$-ferrocene) was coupled by *O*-(7-azabenzotriazol-1-yl)-1,1,3,3-tetramethyluronium hexafluorophosphate (HATU) in the presence of *N*,*N*-diisopropylethylamine (DIEA). After that, the Boc group at the *N*-terminal was removed by treatment with 4 N HCl in dioxane and DL-α-lipoic acid was coupled similarly using HATU and DIEA. SSA24Fc was synthesized differently due to its poor solubility in 4 N HCl dioxane solution. Boc-$(Ala\text{-}Aib)_4$-OBzl was modified with DL-α-lipoic acid after similar deprotection of the Boc group, and then the OBzl group was removed by treatment with a 1 N NaOH aqueous solution in methanol and dioxane. This fragment was coupled to the *N*-terminal of the 16mer having the ferrocene moiety at the *C*-terminal, which was the intermediate for synthesis of SSA16Fc by HATU and DIEA to afford SSA24Fc. All the intermediates were identified by ^{1}H NMR spectroscopy and the final products were further confirmed by FAB mass spectrometry. The purity of each compound was checked by thin-layer chromatography (TLC). The identification data of the final products are shown below.

SSA8Fc TLC [chloroform/methanol (10/1 v/v)]: $R_f = 0.26$, (chloroform/methanol (5/1 v/v)): $R_f = 0.59$, (chloroform/methanol/ammonia water = 13/5/1 v/v/v): $R_f = 0.81$. ^{1}H NMR (400 MHz, $CDCl_3$): δ(ppm) 1.49–1.60 (42H, m, $(CH_2)_3CH_2CO$, $AlaC^{\beta}H_3$, $AibCH_3$), 1.95, 2.50 (2H, m, $SSCH_2CH_2CH$),

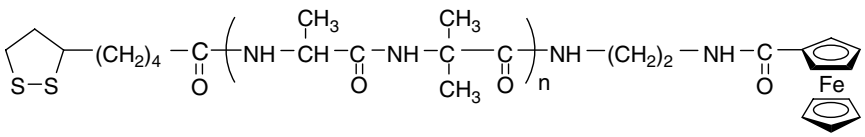

Figure 1 Chemical structures of SSA8Fc, SSA16Fc, and SSA24Fc.

DOI: 10.1002/psc

2.34 (2H, m, $(CH_2)_3CH_2CO$), 3.14 (2H, m, $SSCH_2CH_2CH$), 3.35–3.70 (5H, brm, $SSCH_2CH_2CH$, $NH(CH_2)_2NH$), 3.99 (4H, m, $AlaC^{\alpha}H$), 4.25, 4.90, 4.97 (9H, s, ferrocene-*H*), 6.55, 6.80, 7.26–7.60 (10H, brm, amide-N*H*). MS (FAB, matrix; nitrobenzylalcohol): *m/z* 1085.50 (calcd for $C_{49}H_{76}FeN_{10}O_{10}S_2$ $[(M+H)^+]$ *m/z* 1085.46).

SSA16Fc TLC [chloroform/methanol (10/1 v/v)]: R_f = 0.27, [chloroform/methanol (5/1 v/v)]: $R_f = 0.63$, (chloroform/methanol/ammonia water = 13/5/1 v/v/v): $R_f = 0.83$. ^{1}H NMR (400 MHz, $CDCl_3$): δ(ppm) 1.35–1.70 (78H, m, $(CH_2)_3CH_2CO$, $AlaC^{\beta}H_3$, $AibCH_3$), 1.91, 2.44 (2H, m, $SSCH_2CH_2CH$), 2.32 (2H, t, $(CH_2)_3CH_2CO$), 3.13 (2H, m, $SSCH_2CH_2CH$), 3.40–3.70 (5H, brm, $SSCH_2CH_2CH$, $NH(CH_2)_2NH$), 3.95 (8H, m, $AlaC^{\alpha}H$), 4.22, 4.88, 5.04 (9H, s, ferrocene-*H*), 7.55–8.10 (18H, brm, amide-N*H*). MS (FAB, matrix; nitrobenzylalcohol): *m/z* 1709.82 (calcd for $C_{77}H_{125}FeN_{18}O_{18}S_2$ $[(M+H)^+]$ *m/z* 1709.82).

SSA24Fc TLC [chloroform/methanol (10/1 v/v)]: R_f = 0.24, [chloroform/methanol (5/1 v/v)]: $R_f = 0.57$, (chloroform/methanol/ammonia water = 13/5/1 v/v/v): $R_f = 0.84$. ^{1}H NMR (400 MHz, $CDCl_3$): δ(ppm) 1.35–1.75 (114H, m, $(CH_2)_3CH_2CO$, $AlaC^{\beta}H_3$, $AibCH_3$), 1.90, 2.50 (2H, m, $SSCH_2CH_2CH$), 2.32 (2H, brm, $(CH_2)_3CH_2CO$), 3.13 (2H, m, $SSCH_2CH_2CH$), 3.35–3.75 (5H, brm, $SSCH_2CH_2CH$, $NH(CH_2)_2NH$), 3.95 (12H, m, $AlaC^{\alpha}H$), 4.22, 4.86, 5.04 (9H, s, ferrocene-*H*), 7.45–8.15 (26H, brm, amide-N*H*). MS (FAB, matrix; nitrobenzylalcohol): *m/z* 2334.23 (calcd for $C_{105}H_{172}FeN_{26}O_{26}S_2$ $[(M+H)^+]$ *m/z* 2334.18).

Circular Dichroism (CD) Spectroscopy

The CD spectra of the peptides in ethanol were recorded on a CD spectropolarimeter (J-600, Jasco, Tokyo) using an optical cell of 0.1 cm optical path length at the residue concentration of 1.0×10^{-3} M at room temperature. The helix contents of the peptides were calculated from Eqn (1) [25].

$$f_H\ (\%) = -([\theta]_{222} + 2340)/30\,300 \qquad (1)$$

f_H and $[\theta]_{222}$ represent the helix content and molar ellipticity in residue concentration at 222 nm.

Preparation of SAMs

A slide glass was cleaned by sulfonic acid and rinsed with water and methanol. A gold substrate was prepared by vapor deposition of chromium and then gold (99.99%) onto the slide glass by a vacuum deposition system (N-KS350, Osaka Vacuum, Osaka). The thicknesses of the chromium and gold layers, monitored by a quartz oscillator, were approximately 300 and 2000 Å, respectively. The prepared gold substrate was immediately used for self-assembling. The gold substrate was incubated in an ethanol solution of the helical peptide (0.1 mM) for 24 h. After incubation, the substrate was rinsed thoroughly with appropriate solvents to remove physisorbed molecules: SSA8Fc SAM with ethanol, SSA16Fc SAM with chloroform, and then chloroform/methanol (v/v = 1/1) and SSA24Fc SAM with chloroform and then chloroform/methanol (twice). After rinsing, the substrate was dried in a steam of dry N_2 and in vacuum for 15 min.

Characterization of Monolayers

IRRAS spectra were recorded on an FT-IR spectrometer (Nicolet 6700 FT-IR, Thermo Fisher Scientific, MA) at room temperature with a reflection attachment (RMA-1DG/VRA, Harrick, NY). The incident angle was set at 85° from the surface normal. The number of interferogram accumulations was 500. Molecular orientation of the peptide monolayer was examined from the amide I/II absorbance ratio in the spectrum according to Eqn (2) assuming uniform orientation of the helix axis around the surface normal [26,27].

$$I_1/I_2 = 1.5[(3\ \cos^2\gamma - 1) \times (3\ \cos^2\theta_1 - 1) + 2] / [(3\ \cos^2\gamma - 1) \times (3\ \cos^2\theta_2 - 1) + 2] \qquad (2)$$

I_i, γ, and θ_i ($i = 1$ or 2 corresponds to amide I or amide II) represent the observed absorbance, the tilt angle of helical axis from the surface normal, and the angle between the transition moment and the helix axis, respectively. The values of the θ_1 and θ_2 were taken to be 39° and 83° (3_{10}-helix) or 75° (α-helix), respectively [28,29].

Ellipsometry was carried out on an auto-ellipsometer (DHA-OLX/S, Mizojiri Optical, Tokyo) at room temperature to determine the thicknesses of the monolayers. A helium–neon laser at a wavelength of 632.8 nm was used as the incident light, and its incident angle was set at 65°. The complex optical constant of the monolayer was assumed to be $1.50 + 0.00\,i$. The thickness of the monolayer was calculated automatically by using an equipped program. The thickness was measured in more than five different spots on the substrate and the results were averaged.

Electrochemical Measurements (CV, CA, and EIS)

Electrochemical experiments were performed by a voltammetric analyzer (model 604, BAS, Tokyo) at room temperature with a three-electrode system with the monolayer-modified gold substrate as the working electrode, Ag/AgCl in a 3 M NaCl aqueous solution as the reference electrode, and a platinum wire as the auxiliary electrode. Milli-Q water was used to prepare the solutions. The solutions were flushed with N_2 for 15 min prior to the experiments. All the applied potentials on the working electrode reported here are with respect to the reference electrode. The area of the working electrode exposed to the electrolyte solution was 0.9–1.1 cm^2. The uncompensated resistance of the cell was estimated to be *ca* 4 ohm by ac voltammetry. The blocking experiment by CV to examine packing of the monolayers was carried out in a 1 mM $K_4[Fe(CN)_6]$ and 1 M KCl aqueous solution. All the remaining experiments were carried out in a 1 M $HClO_4$ aqueous solution. In CA, the time constant in the current follower of the potentiostat was set at 10^{-4} s. The potential was stepped from 0.44 (formal oxidation potential) − overpotential (V) to 0.44 + overpotential (V) at time zero. EIS was performed with a dc voltage of 50 mV at frequency ranging from 10^5 to 10^{-2} Hz. The Bode plot obtained at 0 V was fitted by an equivalent circuit [30] consisting of the solution resistance (R_s), monolayer resistance (R_m), and monolayer constant phase element (CPE) [$Z_{CPE} = (1/(Q(i\omega)^n))$] to determine these parameters. In this study, a CPE was used instead of a capacitance to get a better agreement between the experimental and simulated curves by accounting for the

DOI: 10.1002/psc

inhomogeneity of the electrode surface [31,32]. The Bode plot obtained at the formal oxidation potential (0.44 V) was fitted by an equivalent circuit [33,34] consisting of R_s, CPE, and electron-transfer resistance (R_{et}) and capacitance (C_{et}). In this fitting, R_s and CPE obtained at 0 V were used as fixed parameters. The standard electron-transfer rate constant ($k_{et}{}^0$) was determined from R_{et} and C_{et} by Eqn (3).

$$k_{et}{}^0 = 1/(2\ R_{et}\ C_{et}) \tag{3}$$

The impedance data taken at 0 V were also analyzed in terms of capacitance to examine the dielectric constants of the monolayers. Assuming the monolayer as a plate condenser, the relative dielectric constant (ε_m) was determined by Eqn (4) with the obtained capacitance of the monolayer (C_m), the thicknesses determined by ellipsometry (d), the vacuum permittivity (ε_v), and the electrode area (S).

$$\varepsilon_m = C_m d/(\varepsilon_v S) \tag{4}$$

Calculations of Molecular Length, Monolayer Thickness, and Monolayer Surface Density

The molecular lengths of the peptides were calculated by summing up the helix length, linker length, and the size of ferrocene. The helix lengths were estimated with 2.0 Å per residue for a 3_{10}-helix (16 Å for the 8mer) and 1.5 Å per residue for an α-helix (24 and 36 Å for the 16mer and 24mer) [35]. Since the conformation of the linker parts at the *N*- and *C*-terminals is unknown, the half value of the length of the all-trans extended chain was taken as approximation. The peptides have 13 bonds from the gold surface to the ferrocene in the total linker parts. Using 1.25 Å as the length per bond along the chain axis (not bonding direction), the length of the extended chain was *ca* 16 Å. Accordingly, the length of the linker parts was taken to be 8 Å. Ferrocene was assumed to be a sphere with a 6 Å diameter. Finally, the total lengths of the peptides were 30, 38, and 50 Å for the 8mer, 16mer, and 24mer, respectively. The distances between the ferrocene moiety and gold were 24, 32, and 44 Å, respectively. The thicknesses of the monolayers were estimated by (molecular length) × cos(tilt angle from IRRAS).

The monolayer surface densities were estimated from the cross-sectional areas of the helices and the tilt angles. Computational geometry optimization was carried out to determine the cross-sectional areas of 3_{10}-helix and α-helix. The initial geometry of each helix was generated on a CAChe WorkSystem software (ver. 6.1.1, Fujitsu, Tokyo). The dihedral angles of the peptide backbone were set to be $\omega = 180°$, $\phi = -60°$, and $\psi = -30°$ for a 3_{10}-helix, while $\omega = 180°$, $\phi = -70°$, and $\psi = -40°$ for an α-helix. The initial geometry was then optimized by the Molecular Mechanics program 2 (MM2) method and the semiempirical Austin Model 1 (AM1) method by the MOPAC 2002 package on the same program. The obtained cross-sectional areas were 0.69 nm^2 (9.4 Å diameter) and 0.92 nm^2 (10.8 Å diameter) for 3_{10}-helix and α-helix, respectively. Assuming hexagonal packing with a tilt angle of 0°, the surface densities were 2.17×10^{-10} and 1.65×10^{-10} mol cm^{-2}, respectively. The surface density of the monolayer was obtained by multiplying this density by cos(tilt angle from IRRAS).

RESULTS AND DISCUSSIONS

The helical peptides (SSA8Fc, SSA16Fc, and SSA24Fc; Figure 1) were synthesized by the liquid-phase synthesis. The peptide conformation in solution was examined by CD spectroscopy (Figure 2). The 8mer showed a negative peak at 205 along with a shoulder around 225 nm that is characteristic of right-handed 3_{10}-helical conformation [36]. On the other hand, the 16mer and 24mer showed a double-minimum pattern at 208 and 222 nm that is a typical feature of right-handed α-helical conformation. The helix contents were determined to be 68% for the 16mer and 78% for the 24mer from the molar ellipticity at 222 nm.

SAMs were prepared on gold from ethanol solutions of the respective peptides. Molecular orientation was studied by IRRAS spectroscopy (Figure 3). Amide I and II were observed at around 1670 and 1540 cm^{-1}, respectively. These wavenumbers are characteristic of helical conformation [29], showing that the helical structure is retained in the monolayer. The tilt angles of the helices from the surface normal were estimated to be 63°, 43°, and 40° for the 8mer, 16mer, and 24mer, respectively, from the ratio of the amide I and II absorbances. This result suggests that stronger intermolecular hydrophobic and van der Waals interactions among longer helical peptides should align the helices parallel to each other, resulting in more vertical orientation on the surface [27]. On the basis of the tilt angles and the molecular lengths, the monolayer thicknesses were estimated to be 14, 28, and 38 Å for the 8mer, 16mer, and 24mer SAMs, respectively. On the other hand, the experimental thicknesses by ellipsometry were 12, 24, and 30 Å. This good agreement indicates that the peptides form a monolayer on the gold surface.

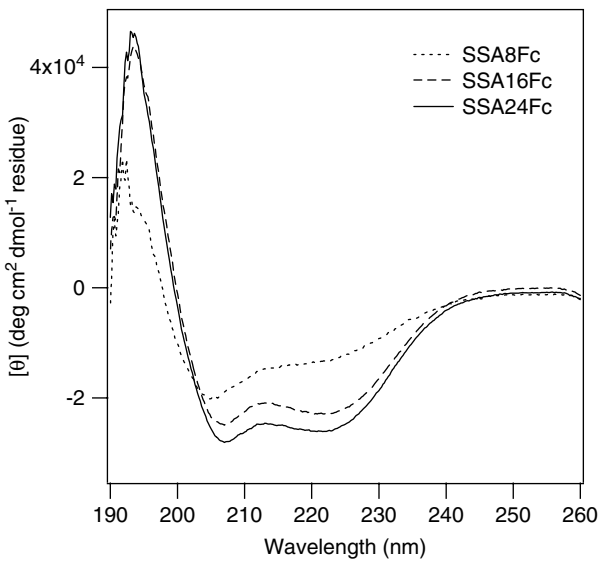

Figure 2 CD spectra of SSA8Fc, SSA16Fc, and SSA24Fc in ethanol.

DOI: 10.1002/psc

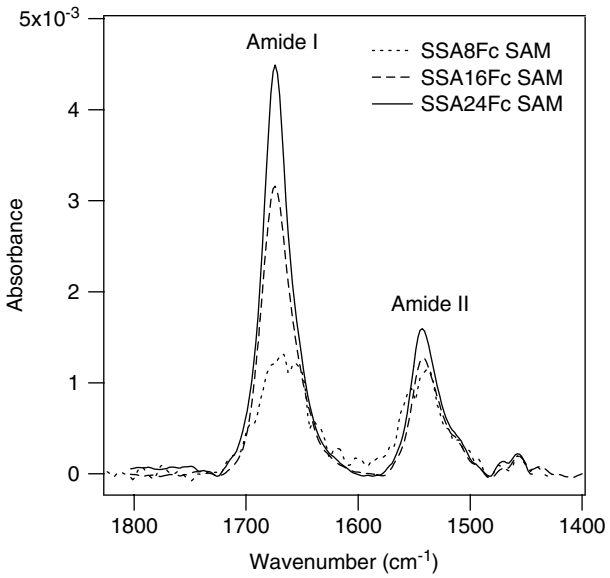

Figure 3 IRRAS spectra of the SSA8Fc, SSA16Fc, and SSA24Fc SAMs.

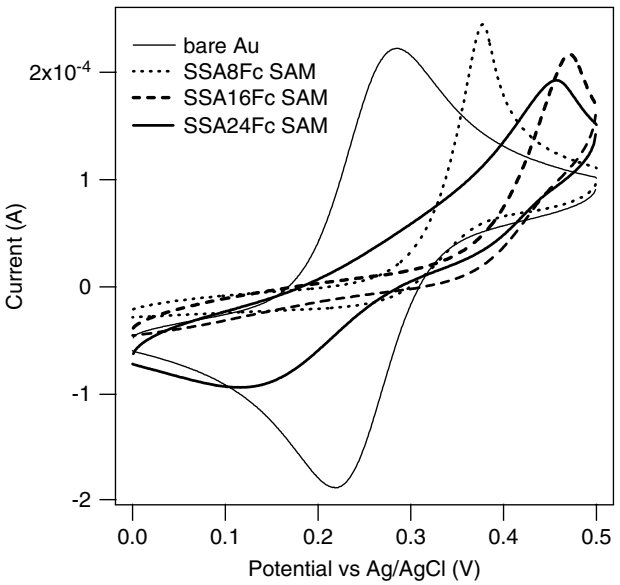

Figure 4 Cyclic voltammograms of a bare gold substrate and the monolayer-modified substrates in a 1 mM $K_4[Fe(CN)_6]$ and 1 M KCl aqueous solution at a scan rate of 0.1 V s^{-1}.

The molecular packing of the monolayers was examined by CV in an aqueous solution containing ferrocyanide ions. The cyclic voltammograms of a control bare gold substrate and the monolayer-modified substrates are shown in Figure 4. Clear redox peaks of $[Fe(CN)_6]^{3-}/[Fe(CN)_6]^{4-}$ were seen in the bare substrate. On the other hand, the ferrocyanide redox peaks were not observed in the 8mer and 16mer SAMs, showing that these monolayers are well packed and do not allow the ferrocyanide ions to diffuse and contact the gold surface, while an oxidation peak of the ferrocene moiety without following reduction was observed (at *ca* 0.38 V for the 8mer SAM and *ca* 0.47 V for the 16mer SAM). This is a typical behavior of a SAM having a ferrocene moiety at the surface [37]. As the oxidized ferrocene moiety is readily reduced by the ferrocyanide ions in the aqueous phase, the reduction peak is not observed. On the other hand, a broad redox peak of ferrocyanide was observed in the 24mer SAM, showing that this monolayer is relatively loosely packed compared to the other monolayers. Since the solubility of the 24mer peptide is low, the peptide did not completely dissolve in the solvent (ethanol) of the preparation solution. This low effective concentration might be not enough to form a well-packed monolayer.

To study the electron transfer between the ferrocene moiety and gold, CV was performed in a perchloric acid solution. Figure 5(a) shows the cyclic voltammograms of the monolayers at a scan rate of 0.5 V s^{-1}. In

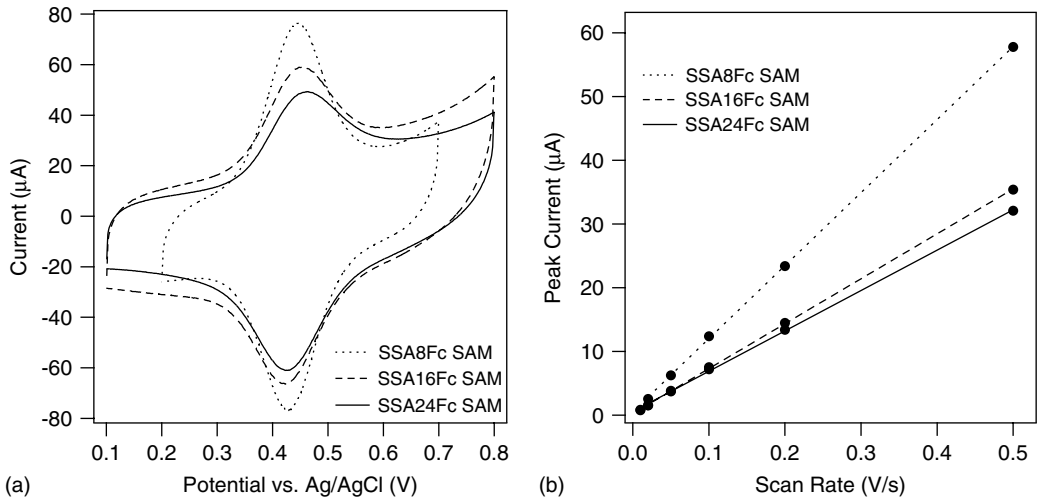

Figure 5 (a) Cyclic voltammograms of the monolayer-modified substrates in a 1 M $HClO_4$ aqueous solution at a scan rate of 0.5 V s^{-1}, and (b) the relationship between the anodic peak currents with the background current subtracted and the scan rates.

DOI: 10.1002/psc

all the monolayers, reversible redox peaks of the ferrocene oxidation were clearly observed. The formal redox potentials were 0.44 V in all the cases. The peak separations were 16, 32, and 36 mV for the 8mer, 16mer, and the 24mer SAMs, respectively. Qualitatively, this indicates that the electron transfer is much faster in the 8mer SAMs than in the other SAMs while the rates are comparable in the 16mer and 24mer SAMs. Figure 5(b) shows the relationship between the anodic peak currents with the background current subtracted and the scan rates. The linear relationship indicates that the electron transfer from the surface-bound ferrocene moiety to gold is responsible for the anodic peak and there is no diffusion-controlled process involved. The surface densities of the ferrocene moiety were calculated by integrating the anodic currents to be 1.4×10^{-10}, 1.1×10^{-10}, and 1.1×10^{-10} mol cm^{-2} for the 8mer, 16mer, and 24mer SAMs, respectively. The surface densities were also estimated from the cross-sectional areas of the helices and the tilt angles determined by IRRAS to be 1.0×10^{-10}, 1.2×10^{-10}, and 1.3×10^{-10} mol cm^{-2}, respectively. They are broadly in agreement with those determined by the cyclic voltammograms. This agreement confirms that the peptides form a uniform monolayer and that all the ferrocene moieties are electrochemically active on the surface.

CA was performed to determine the standard electron-transfer rate constant (k_{et}^0). Time courses of the currents after applying various overpotentials are shown in Figure 6(a), (c), (d) in the form of a semilog plot. The 8mer SAM (Figure 6(a)) shows a linear decay of the current that is characteristic of a first-order electron-transfer reaction between a surface-bound redox species and a metal surface [38–40]. The curves were fitted by a linear function to get the slopes that were plotted against overpotentials (Figure 6(b)) and k_{et}^0 was determined by extrapolation

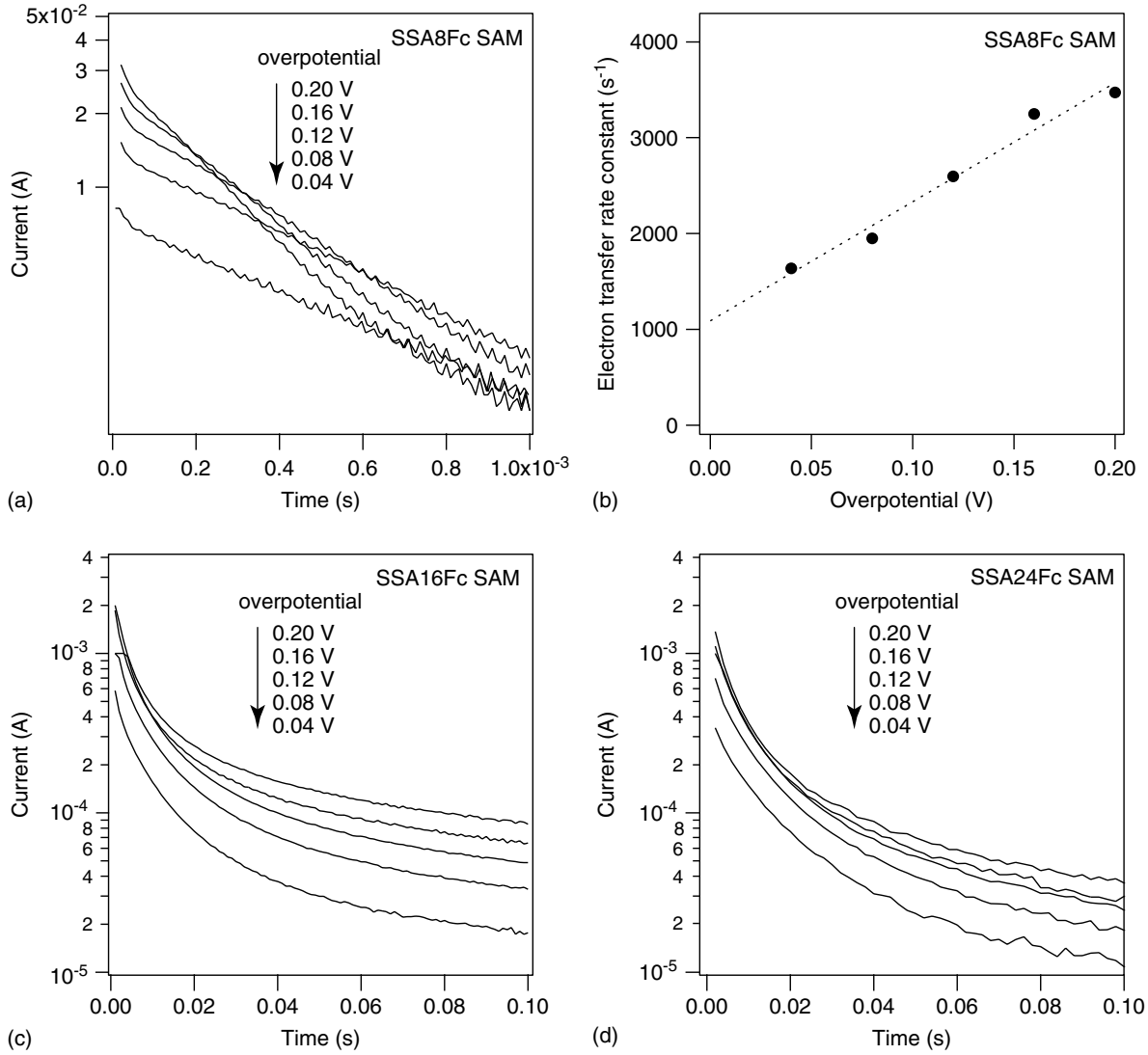

Figure 6 Time courses of the currents at various overpotential in the SSA8Fc (a), SSA16Fc (c), SSA24Fc (d) SAMs, and (b) the plot of the electron-transfer rate constants on overpotentials for the SSA8Fc SAM.

DOI: 10.1002/psc

to the zero overpotential (1100 s^{-1}). Unfortunately, the CA analyses of the 16mer and 24mer SAMs were unsuccessful because a linear region was not found in the current-time curves (Figure 6(c), (d)) probably due to overlapping with background currents of a comparable time constant. Therefore, the k_{et}^0 values were examined by another technique, EIS.

EIS was carried out to determine k_{et}^0 for all the monolayers. The results obtained at 0 and 0.44 V (formal potential of ferrocene oxidation) in the form of a Bode plot (absolute impedance ($|Z|$) and phase *vs* frequency) are shown in Figure 7. The Bode plots at 0 V (Figure 7(a)) were analyzed by an equivalent circuit A [30] to determine the solution resistance (R_s), monolayer resistance (R_m), and monolayer CPE [$Z_{CPE} = (1/(Q(i\omega)^n))$]. Using the obtained R_s and CPE as fixed parameters, the Bode plots at 0.44 V (Figure 7(b)) were analyzed by an equivalent circuit B [33,34] to determine the electron-transfer resistance (R_{et}) and capacitance (C_{et}). Finally, the k_{et}^0 values were determined from R_{et} and C_{et} [$k_{et}^0 = 1/(2\ R_{et}\ C_{et})$]. The fitting parameters for the Bode plots in Figure 7 are summarized in Table 1. The obtained k_{et}^0 value for the 8mer SAM is 2000 s^{-1} that is in the same order as that determined by CA (1100 s^{-1}). For the 16mer and 24mer SAMs, the average values were obtained by more than three separate experiments. They are 64 ± 18 s^{-1} for the 16mer SAM and 50 ± 2 s^{-1} for the 24mer SAM, respectively. These comparable rate constants agree with the qualitative interpretation of the CV peak separations. The impedance data taken at 0 V were also analyzed with a normal capacitance to examine the dielectric constants of the monolayers. From the capacitances and thicknesses of the monolayers, the

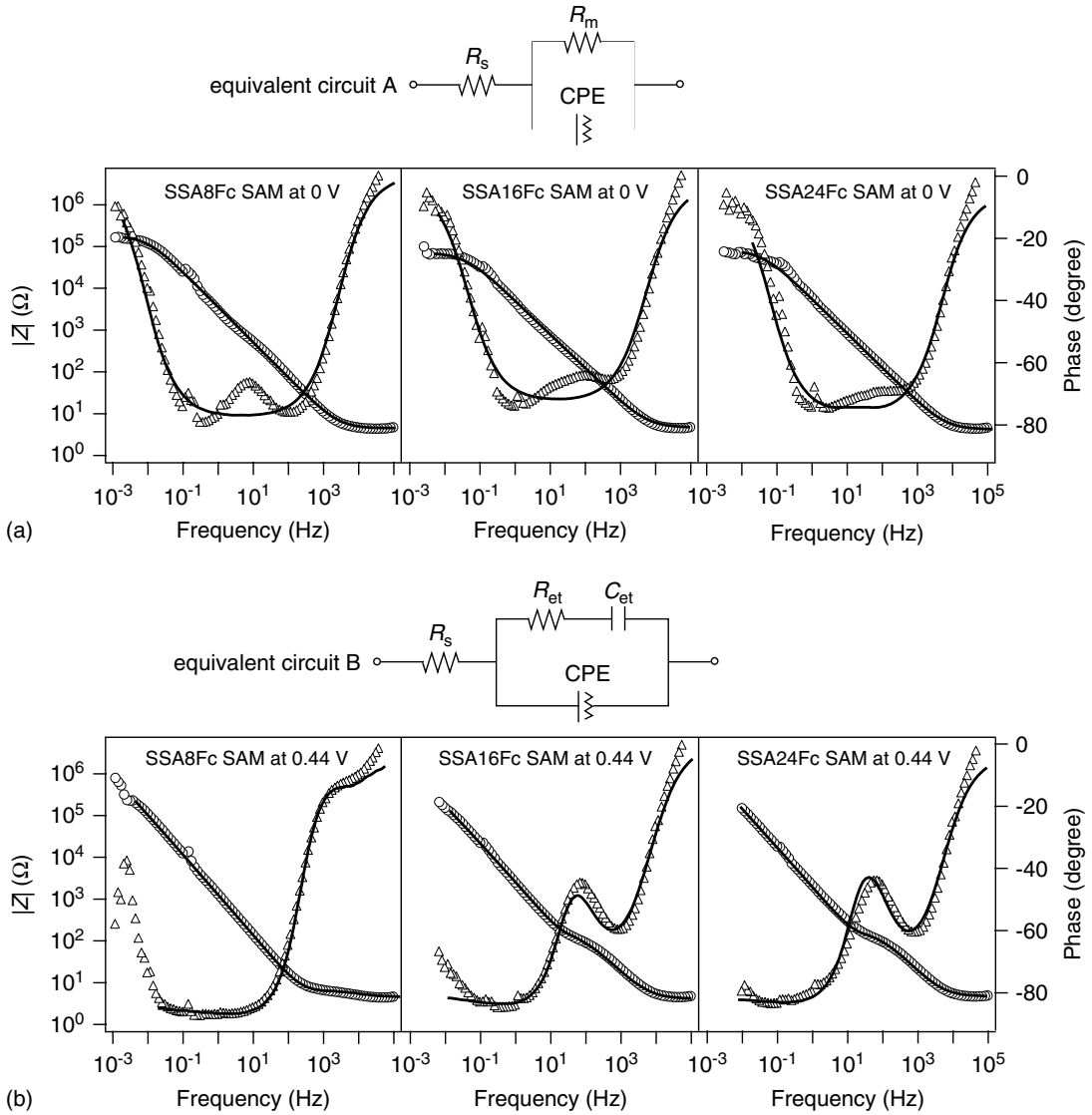

Figure 7 Bode plots for the EIS analyses of the peptide monolayers at 0 V (a) and 0.44 V (b). The open circles and triangles show the experimental absolute impedance ($|Z|$) and phase and the solid lines are the fitting curves. The fitting parameters are summarized in Table 1.

DOI: 10.1002/psc

relative dielectric constants were estimated to be 39, 20, and 45 for the 8mer, 16mer, and 24mer peptide monolayers. For the 24mer peptide monolayer, this result is in line with the result of the blocking experiments. The high dielectric constant is explained by water and electrolytes taken in by the defective sites of the monolayer. On the other hand, a relatively large dielectric constant was also obtained for the 8mer peptide monolayer that did not allow permeation of the redox ions in the blocking experiment. This may infer that this thin monolayer with large tilt is incomplete and contains water molecules and ions near the surface region but does not have vertical defects throughout the layer.

Figure 8 shows the distance dependence of $k_{et}{}^0$ determined by EIS. Figure 8(a) is the plot *versus* the distance between the ferrocene moiety and gold along the molecular axis, while Figure 8(b) is the plot *versus* the monolayer thickness determined by ellipsometry. If the electron transfer occurs intramolecularly along the molecular axis (Figure 8(a)), the β value from the 8mer to 16mer is 0.45 $Å^{-1}$. This value is smaller than the values reported by Sisido and co-workers (0.66 $Å^{-1}$) [9] and by Sek and co-workers (0.50 $Å^{-1}$) [18]. In contrast, the β value from the 16mer to 24mer is only 0.02 $Å^{-1}$. This extraordinarily small decay factor cannot be explained by a tunneling mechanism. On the other hand, if the electron transfer occurs intermolecularly along the surface normal direction (Figure 8(b)), the β values are 0.29 $Å^{-1}$ from the 8mer to 16mer, and 0.04 $Å^{-1}$ from the 16mer to 24mer, respectively. The latter value is also too small for a tunneling mechanism. Whether an electron is transferred along the molecule or along the surface normal, tunneling may be operative in the 8mer SAM due to the short distance, but there should be another mechanism other than tunneling that is responsible for the long-range electron transfer in the 16mer and 24mer SAMs.

Maran and co-workers have emphasized that the cooperativity of hydrogen bonding is important for the weak distance dependence of electron transfer through a helical peptide [21,22]. They explained as follows. As a peptide becomes longer, the number of hydrogen bonds increases to open new electron tunneling pathways. At the same time, the structure becomes solid and the frontier molecular orbital levels of the bridge shift (in their case, the level of lowest unoccupied molecular orbital (LUMO) goes down) to accelerate the electron tunneling. We agree with their opinion for the short peptides they used (0mer to 6mer). However, for much longer peptides we used in the present study, their explanation cannot hold because the number of tunneling pathways stays the same and the integrity of the helical conformation should retain for these long peptides. In fact, the difference in helix contents between the 16mer and 24mer is only 10% (Figure 2). This small difference in the hydrogen bond cooperativity cannot explain the observed anomalously small decay constant from the 16mer to 24mer. On the other hand, Kraatz and co-workers have

Table 1 The fitting parameters for the Bode plots shown in Figure 7

	SSA8Fc SAM	SSA16Fc SAM	SSA24Fc SAM
R_s (Ω)	4.16	4.18	4.31
R_m (Ω)	1.75×10^5	7.66×10^4	6.68×10^4
CPE Q (Ω^{-1} s^n)	5.60×10^{-5}	4.13×10^{-5}	3.00×10^{-5}
CPE n	0.856	0.820	0.856
R_{et} (Ω)	3.17	187	178
C_{et} (F)	7.73×10^{-5}	3.37×10^{-5}	5.42×10^{-5}
$k_{et}{}^0$ (s^{-1})	2040	79.6	52.0

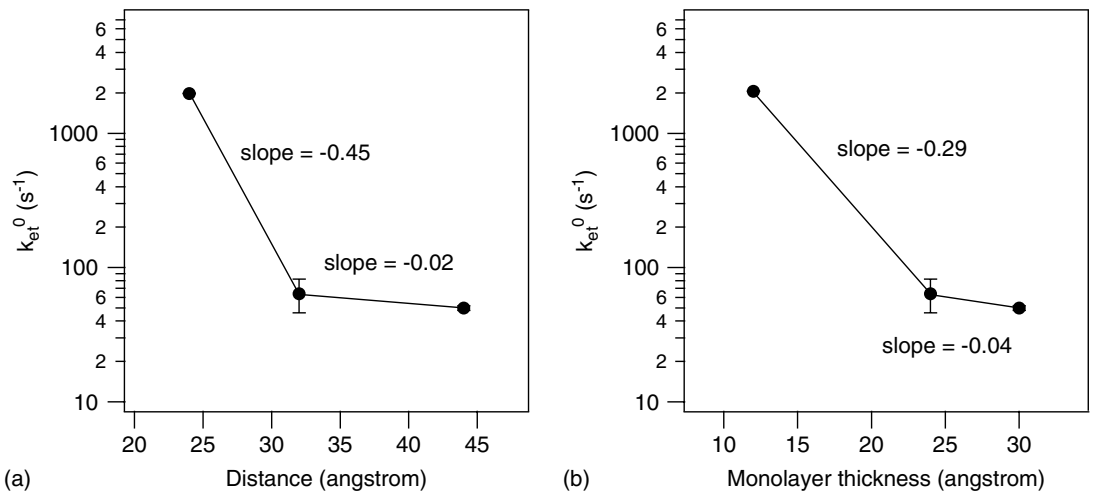

Figure 8 Plots of the standard electron-transfer rate constants ($k_{et}{}^0$) on the distances along the molecular axis (a) and on the monolayer thicknesses (b).

DOI: 10.1002/psc

pointed out the importance of molecular dynamics on peptide electron transfer [14]. They suggested a conformationally gated electron-transfer mechanism in which the peptide conformation thermally fluctuates and accordingly, some specific motions may promote the electronic interaction between adjacent electronic sites along the peptide. When the 24mer SAM was prepared from ethanol/chloroform (4/1 v/v) and with inadequate solvent rinse, the SAM was better packed than that was prepared from ethanol, probably due to partial insertion of the peptide in antiparallel manner and nonspecific adsorption on the surface (tilt angle 55° and thickness 65 Å). The CA and EIS gave 6–12 times smaller k_{et}^0 values (8.3 s^{-1} from CA, 4.2 s^{-1} from EIS). This comparison suggests that a less packed environment allows conformational fluctuation of a helical peptide to promote electron transfer. Let us consider what kind of fluctuation made this difference. In the above-mentioned blocking experiment, the peak areas of $[Fe(CN)_6]^{3-}/[Fe(CN)_6]^{4-}$ redox for the 24mer monolayer prepared from ethanol were about 20% of those for the bare substrate (Figure 4) meaning that the uncovered surface was about 20%. Assuming homogeneous distribution of the bare surface, each peptide molecule has a free space of 0.26 nm^2 (the molecular area of the 24mer helical peptide with a tilt angle of 40° is 1.32 nm^2. 1.32 $nm^2 \times 0.2 = 0.26$ nm^2). This free space is too small to allow lateral fluctuations of the rigid helical peptides with large tilting or folding to bring the ferrocene moiety close to the gold surface. Only vertical fluctuation along the helix axis may be possible. However, it is not plausible that the 24mer peptide shrinks to the length of the 16mer peptide to show a comparable electron tunneling rate. Therefore, we consider that conformational fluctuation along the helix axis should promote the charge hopping process among the amide groups because of enhancement of the electron coupling between the amide groups probably with a certain vibration mode, and so on. Moreover, even with the k_{et}^0 values of the better packed 24mer peptide monolayer, the β value is still as small as 0.2 $Å^{-1}$ from the 16mer to 24mer that may not be explained by electron tunneling. To get more information on molecular dynamics, the temperature dependence of the electron transfer will be examined.

If the electron transfer is operated by the hopping mechanism with the amide groups as the hopping site, the rate-determining step should be electron transfer from the nearest amide group to gold (hole injection from gold). The LUMO level of an amide group is so high that electron tunneling via the LUMO level at the interface is excluded. However, the most questionable point for the hopping mechanism is the large energy gap between the oxidation potential of the amide group and the Fermi level of gold. The ionization potential of an amide group in a peptide chain under vacuum is reported to be *ca* 9 eV [41]. Using an empirical linear relationship between the ionization potential in vacuum and oxidation potential in solvent in the literature [formal potential *vs* $Ag/AgNO_3$ electrode in acetonitrile = 0.92 × (ionization potential) − 6.2] [42], the oxidation potential of an amide group is *ca* 2.4 V *versus* Ag/AgCl reference electrode in water. When the potential of gold is set at the formal potential of ferrocene oxidation (0.44 V), the energy gap between the amide oxidation potential and the gold Fermi level is *ca* 2.0 eV (assuming that the potential drops at the metal/organic interface). This energy gap is too large for reasonable electron transfer. However, it has recently been reported that there is an interfacial state produced by hybridization of the orbitals of the sulfur and gold atoms at 1.0–1.5 eV below the Fermi level [43,44]. If this state works as a stepping stone for an electron from the amide group to gold, the energy gap is reduced to be 0.5–1.0 eV. On top of that, image charge formation inside the metal should stabilize the amide cation radical and hence, decrease the oxidation potential to reduce the gap more [45]. To examine this hypothesis, we are going to study helical peptide monolayers prepared on other metals such as silver and platinum. The difference in work functions should change the energy gap of the reaction and should remarkably influence the electron-transfer rate if it is operated by the hopping mechanism.

CONCLUSIONS

SAMs were prepared on gold from helical peptides having ferrocene moiety at the terminal. Three different lengths of peptides were used, namely, 8mer, 16mer, and 24mer. Each peptide formed a uniform monolayer with upright orientation, confirmed by infrared spectroscopy and ellipsometry. CV showed that the electron transfer from the ferrocene moiety to gold occurs in all the cases. This is the first example to study long-range electron transfer through a long 24mer helical peptide. CA and EIS gave the standard rate constants. Surprisingly, the decay factor from the 16mer to 24mer is extraordinarily small, 0.02–0.04 $Å^{-1}$. This small decay factor cannot be explained by a tunneling mechanism even by taking into account hydrogen-bonding cooperativity and molecular dynamics. We thus concluded that a hopping mechanism should be responsible for this long-range electron transfer. Dependencies of the electron transfer on temperatures and metal work functions are going to be examined along with theoretical calculations of the electron transfer rates to prove the hopping mechanism.

Acknowledgements

This work was supported by Grant-in-Aid for Young Scientists B (16750098) and 21st century COE program,

DOI: 10.1002/psc

COE for a United Approach to New Materials Science from the Ministry of Education, Culture, Sports, Science, and Technology, Japan, and by Grant-in-Aids for Exploratory Research (17655098) and for Scientific Research B (15350068) from Japan Society for the Promotion of Science.

REFERENCES

1. Mayo SL, Ellis WR, Crutchley RJ, Gray HB. Long-range electron-transfer in heme-proteins. *Science* 1986; **233**: 948–952.
2. Beratan DN, Onuchic JN, Winkler JR, Gray HB. Electron-tunneling pathways in proteins. *Science* 1992; **258**: 1740–1741.
3. Langen R, Chang IJ, Germanas JP, Richards JH, Winkler JR, Gray HB. Electron-tunneling in proteins–coupling through a beta-strand. *Science* 1995; **268**: 1733–1735.
4. Isied SS. Long-range electron-transfer in peptides and proteins. *Prog. Inorg. Chem.* 1984; **32**: 443–517.
5. Shin YGK, Newton MD, Isied SS. Distance dependence of electron transfer across peptides with different secondary structures: The role of peptide energetics and electronic coupling. *J. Am. Chem. Soc.* 2003; **125**: 3722–3732.
6. Hol WGJ. The role of the alpha-helix dipole in protein function and structure. *Prog. Biophys. Mol. Biol.* 1985; **45**: 149–195.
7. Vassilian A, Wishart JF, Vanhemelryck B, Schwarz H, Isied SS. Electron-transfer across polypeptides.6. Long-range electron-transfer in osmium-ruthenium binuclear complexes bridged with oligoproline peptides. *J. Am. Chem. Soc.* 1990; **112**: 7278–7286.
8. Ogawa MY, Wishart JF, Young ZY, Miller JR, Isied SS. Distance dependence of intramolecular electron-transfer across oligoprolines in [(bpy)2ruiil-(pro)n-coiii (nh3) 5] 3+, n = 1–6 – different effects for helical and nonhelical polyproline-ii structures. *J. Phys. Chem.* 1993; **97**: 11456–11463.
9. Sisido M, Hoshino S, Kusano H, Kuragaki M, Makino M, Sasaki H, Smith TA, Ghiggino KP. Distance dependence of photoinduced electron transfer along alpha-helical polypeptides. *J. Phys. Chem. B* 2001; **105**: 10407–10415.
10. Morita T, Kimura S. Long-range electron transfer over 4 nm governed by an inelastic hopping mechanism in self-assembled monolayers of helical peptides. *J. Am. Chem. Soc.* 2003; **125**: 8732–8733.
11. Watanabe J, Morita T, Kimura S. Effects of dipole moment, linkers, and chromophores at side chains on long-range electron transfer through helical peptides. *J. Phys. Chem. B* 2005; **109**: 14416–14425.
12. Galka MM, Kraatz HB. Electron transfer studies on self-assembled monolayers of helical ferrocenoyl-oligoproline-cystamine bound to gold. *Chemphyschem* 2002; **3**: 356–359.
13. Kraatz HB, Bediako-Amoa I, Gyepi-Garbrah SH, Sutherland TC. Electron transfer through h-bonded peptide assemblies. *J. Phys. Chem. B* 2004; **108**: 20164–20172.
14. Mandal HS, Kraatz HB. Electron transfer across alpha-helical peptides: potential influence of molecular dynamics. *Chem. Phys.* 2006; **326**: 246–251.
15. Sek S, Tolak A, Misicka A, Palys B, Bilewicz R. Asymmetry of electron transmission through monolayers of helical polyalanine adsorbed on gold surfaces. *J. Phys. Chem. B* 2005; **109**: 18433–18438.
16. Xiao XY, Xu BQ, Tao NJ. Conductance titration of single-peptide molecules. *J. Am. Chem. Soc.* 2004; **126**: 5370–5371.
17. Sek S, Swiatek K, Misicka A. Electrical behavior of molecular junctions incorporating alpha-helical peptide. *J. Phys. Chem. B* 2005; **109**: 23121–23124.
18. Sek S, Misicka A, Swiatek K, Maicka E. Conductance of alpha-helical peptides trapped within molecular junctions. *J. Phys. Chem. B* 2006; **110**: 19671–19677.
19. Long YT, Abu-Rhayem E, Kraatz HB. Peptide electron transfer: more questions than answers. *Chem.-A Eur. J.* 2005; **11**: 5186–5194.
20. Adams DM, Brus L, Chidsey CED, Creager S, Creutz C, Kagan CR, Kamat PV, Lieberman M, Lindsay S, Marcus RA, Metzger RM, Michel-Beyerle ME, Miller JR, Newton MD, Rolison DR, Sankey O, Schanze KS, Yardley J, Zhu XY. Charge transfer on the nanoscale: current status. *J. Phys. Chem. B* 2003; **107**: 6668–6697.
21. Antonello S, Formaggio F, Moretto A, Toniolo C, Maran F. Anomalous distance dependence of electron transfer across peptide bridges. *J. Am. Chem. Soc.* 2003; **125**: 2874–2875.
22. Polo F, Antonello S, Formaggio F, Toniolo C, Maran F. Evidence against the hopping mechanism as an important electron transfer pathway for conformationally constrained oligopeptides. *J. Am. Chem. Soc.* 2005; **127**: 492–493.
23. Malak RA, Gao ZN, Wishart JF, Isied SS. Long-range electron transfer across peptide bridges: The transition from electron superexchange to hopping. *J. Am. Chem. Soc.* 2004; **126**: 13888–13889.
24. Otoda K, Kitagawa Y, Kimura S, Imanishi Y. Chain-length dependent transition of 3(10)- to alpha-helix of boc-(ala-aib) (n)-ome. *Biopolymers* 1993; **33**: 1337–1345.
25. Chen YH, Yang JT, Martinez HM. Determination of secondary structures of proteins by circular-dichroism and optical rotatory dispersion. *Biochemistry* 1972; **11**: 4120–4131.
26. Gremlich HU, Fringeli UP, Schwyzer R. Conformational-changes of adrenocorticotropin peptides upon interaction with lipid-membranes revealed by infrared attenuated total reflection spectroscopy. *Biochemistry* 1983; **22**: 4257–4264.
27. Miura Y, Kimura S, Imanishi Y, Umemura J. Formation of oriented helical peptide layers on a gold surface due to the self-assembling properties of peptides. *Langmuir* 1998; **14**: 6935–6940.
28. Tsuboi M. Infrared dichroism and molecular conformation of alpha-form poly-gamma-benzyl-l-glutamate. *J. Polym. Sci.* 1962; **59**: 139–153.
29. Kennedy DF, Crisma M, Toniolo C, Chapman D. Studies of peptides forming 3(10)-helices and alpha-helices and beta-bend ribbon structures in organic solution and in model biomembranes by fourier-transform infrared-spectroscopy. *Biochemistry* 1991; **30**: 6541–6548.
30. Steinem C, Janshoff A, Ulrich WP, Sieber M, Galla HJ. Impedance analysis of supported lipid bilayer membranes: A scrutiny of different preparation techniques. *Biochim. Biophys. Acta* 1996; **1279**: 169–180.
31. Wu XZ, Zhang WZ, Hou Y. Assessing nonlinearity in impedance models–the model characteristics of an equivalent-circuit with a cpe. *J. Electroanal. Chem.* 1995; **398**: 1–4.
32. Protsailo LV, Fawcett WR. Studies of electron transfer through self-assembled monolayers using impedance spectroscopy. *Electrochim. Acta* 2000; **45**: 3497–3505.
33. Yamada T, Nango M, Ohtsuka T. Potential modulation reflectance of manganese halogenated tetraphenylporphyrin derivatives assembled on gold electrodes. *J. Electroanal. Chem.* 2002; **528**: 93–102.
34. Creager SE, Wooster TT. A new way of using ac voltammetry to study redox kinetics in electroactive monolayers. *Anal. Chem.* 1998; **70**: 4257–4263.
35. Benedetti E, Di Blasio B, Pavone V, Pedone C, Santini A, Crisma M, Toniolo C. In *Molecular Conformation and Biological Interactions*, Balaram P, Ramaseshan S (eds). Indian Academy of Science: Bangalore, 1991; 497–502.
36. Toniolo C, Polese A, Formaggio F, Crisma M, Kamphuis J. Circular dichroism spectrum of a peptide 3(10)-helix. *J. Am. Chem. Soc.* 1996; **118**: 2744–2745.
37. Niwa M, Morikawa M, Higashi N. Controllable orientation of helical poly(l-glutamic acid) rods through macrodipole interaction on gold surfaces and vectorial electron transfer. *Angew. Chem. Int. Ed. Engl.* 2000; **39**: 960–963.

38. Finklea HO, Ravenscroft MS, Snider DA. Electrolyte and temperature effects on long-range electron-transfer across self-assembled monolayers. *Langmuir* 1993; **9**: 223–227.
39. Finklea HO, Hanshew DD. Electron-transfer kinetics in organized thiol monolayers with attached pentaammine(pyridine)ruthenium redox centers. *J. Am. Chem. Soc.* 1992; **114**: 3173–3181.
40. Sek S, Palys B, Bilewicz R. Contribution of intermolecular interactions to electron transfer through monolayers of alkanethiols containing amide groups. *J. Phys. Chem. B* 2002; **106**: 5907–5914.
41. Weinkauf R, Schanen P, Metsala A, Schlag EW, Burgle M, Kessler H. Highly efficient charge transfer in peptide cations in the gas phase: Threshold effects and mechanism. *J. Phys. Chem.* 1996; **100**: 18567–18585.
42. Miller LL, Mayeda EA, Nordblom GD. Simple, comprehensive correlation of organic oxidation and ionization potentials. *J. Org. Chem.* 1972; **37**: 916–&.
43. Tomfohr JK, Sankey OF. Complex band structure, decay lengths, and fermi level alignment in simple molecular electronic systems. *Phys. Rev., B* 2002; **65**: 245105-1-12.
44. Beerbom MM, Gargagliano R, Schlaf R. Determination of the electronic structure of self-assembled l-cysteine/au interfaces using photoemission spectroscopy. *Langmuir* 2005; **21**: 3551–3558.
45. Petrov EG, May V, Hanggi P. Controlling electron transfer processes through short molecular wires. *Chem. Phys.* 2002; **281**: 211–224.

DOI: 10.1002/psc